LARGE-SCALE SPIRAL STRUCTURES IN TURBULENT NATURAL CONVECTION BETWEEN TWO VERTICAL PLATES

Minghao Wang Song Fu Guanghua Zhang
Department of Engineering Mechanics,
Tsinghua University
Beijing, 100084, China
wmh99@mails.tsinghua.edu.cn, fs-dem@tsinghua.edu.cn, zhanggh@tsinghua.edu.cn

ABSTRACT

For the turbulent thermal convection between two vertical plates, it is observed that the flow can generate large-scale spiral structures. Basing on the DNS data, this type of large-scale structures is studied in spectrum space and in physical space. By FFT of fluctuant velocity and kinetic energy, it is shown that the energy-intensive scale in the flow are about 0.01 in nondimensional time scale and 1.4 in nondimensional space scale, which are in accordance with the observation of the structures described useing streamlines. Further, the instantaneous flow patterns and the time evolution of such spiral structure is illustrated in the paper. For the emergence of the spiral structures, The role of helicity in the flow is to suppress the energy cascade of turbulence, reducing the dissipation, and hence preserving the topological structure of the large-scale spiral flow for a significantly long time interval.

INTRODUCTION

The natural convection between two parallel plates can be categorized, typically, in two types. One is the well-known Rayleigh-Bénard convection in which the plates are horizontal with the bottom plate having higher temperature than the top. In this Rayleigh-Bénard convection the mean temperature gradient is in the direction parallel and opposite to the gravity force. The other is between two vertical plates, which is studied here (Fig.1), with the mean temperature gradient perpendicular to the gravity force in the horizontal direction. In this study the former is referred to as the natural convection of the first kind while the latter is called the natural convection of the second kind. Many of the existing studies on the turbulent coherent structures have been associated with Rayleigh-Bénard convection. For instance, in the "hard turbulence" regime at sufficiently high Rayleigh numbers, Cortese and Balachandar (1993) investigated the vortical nature of thermal plumes through numerical simulation. Their work revealed the existence of the up and down motions of the thermal plumes associated with significant vertical vorticity, of which the horizontal scale is nearly an order of magnitude smaller than the depth of the convection layer. As opposed to the mechanism of large-scale instability, Cortese and Balachandar (1993) proposed that the physical mechanism responsible for these differently scaling structures is the interaction between buoyancy induced vertical flow and shear associated with the large-scale horizontal cellular motions which exist instantaneously near the top and bottom boundaries.

However, only a few published works have been contributed to the understanding of the coherent structures in the natural convection of the second kind. Boudjemadi

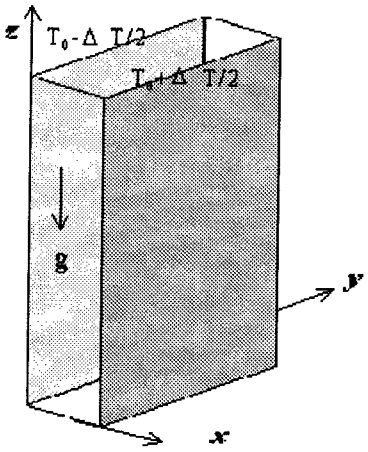

Figure 1: Schematic of the thermal convection between two vertical plates.

et al. (1997) and Phillips (1996) performed DNS studies on this flow at Rayleigh number $Ra = 4.6 \times 10^4$ and 1.28×10^5, respectively. The main focus there was on the statistical mean flow behaviour rather than on the large-scale coherent structures. Versteegh and Nieuwstadt (1999) investigated the same flow through DNS with a somewhat larger computational domain. It was realized in that work that better agreement with the experimental data of Dafa'alla and Betts (1996) can be achieved with the larger computational domain size. Using the DNS data, Versteegh and Nieuwstadt(1997) also studied the coherent structures present in the flow and argued that the most unstable flow pattern in the transition regime could still be recognized in the turbulent flow at a Rayleigh number in the range of $5.4 \times 10^5 - 5.0 \times 10^6$. In the present work, Versteegh and Nieuwstadt's case (1999) with $Ra = 5.4 \times 10^5$ is further scrutinized through DNS. It is observed that the large-scale coherent spiral structures generally occur even at "soft turbulence" with relatively lower Rayleigh number. The present study attempts to highlight the characteristics of the spiral structures in terms of flow visualization, helicity and spectral analysis.

GOVERNING EQUATIONS AND COMPUTATIONAL METHOD

The flow induced by the thermal convection can be described by the well-known Boussinesq equations. In the non-dimensional forms they are written as follows:

$$\frac{\partial u_i}{\partial x_i} = 0 \qquad (1)$$

$$\frac{Du_i}{Dt} = -\frac{\partial p}{\partial x_i} + Pr\frac{\partial^2 u_i}{\partial x_j \partial x_j} + RaPr(T - T_0)\delta_{3i} \quad (2)$$

$$\frac{DT}{Dt} = \frac{\partial^2 T}{\partial x_j \partial x_j} \quad (3)$$

where $Ra = \beta g \Delta T h^3/\kappa\nu$ is the Rayleigh number, $Pr = \nu/\kappa$ the Prandtl number, and h the spacing between the two plates. The coefficients β, ν and κ are the thermal expansion coefficient, kinematic viscosity and thermal diffusion coefficient of the fluid respectively. The subscript indices i and j (=1, 2, 3) in the above equations correspond to component in x, y, z respectively. δ_{ij} is the Kronecker delta. As Pr is set to constant, the only characteristic parameter is Ra. All the variables in this paper are non-dimensional with h being the length scale, κ/h the velocity scale and h^2/κ the time scale.

According to Ruth's linear instability analysis (Ruth,1979), the lowest critical Rayleigh number at which the flow starts to lose stability is about 5710 when $Pr = 0.71$. In the present numerical simulation the Prandtl number is taken as 0.71 and $Ra = 5.4 \times 10^5$. The flow is therefore well above the instability threshold and has become turbulent. Eqs. (1)~(3) are solved numerically in a computational domain of the size $L_x \times L_y \times L_z = 1 \times \pi \times 2\pi$ in the normal, spanwise and streamwise directions. For the boundary conditions, the no-slip condition is applied to the surfaces of the two vertical plates for velocity and the isotherm condition for temperature. In the homogeneous y and z directions, the flow is assumed periodic. A cartesian grid system with the number of grid points $N_x \times N_y \times N_z = 96 \times 90 \times 206$ is adopted. In the y- and z-direction the grid spacing is uniform, whereas in the x-direction the grid spacing is non-uniform with the minimum size near the wall and the maximum size near the centerline.

From Kolmogorov hypothesis, it can be estimated that the smallest length and time scales in the flow are respectively 0.017 and 1×10^{-3}. The numerical technique applied here is a finite-volume scheme with second-order discretization for both the non-linear advection and the viscous diffusion terms. The time-stepping method is an implicit scheme of second-order accuracy. It is considered that such an accuracy is sufficient for the description of the large-scale flow patterns. After a sufficiently long time of computation starting from the initial condition, about 0.6 non-dimensional time length, the flow reaches a statistically steady state. The mean velocity and mean temperature distributions of the flow are shown in Fig.2.

In the DNS of the present flow, Boudjemadi *et al* (1997) and Versteegh and Nieuwstadt (1999) adopted very different sizes of the computational domain. The latter authors employed much larger computational domain than the former and find significant improvement in the results. The present computational domain is only a quarter of the one used by Versteegh and Nieuwstadt to save computational resources but significantly larger than the one employed by Boudjemadi *et al.* In order to validate whether the present computational domain is sufficient, two-point correlation coefficients in streamwise and spanwise directions are plotted in fig.3. The results are obtained with about 1000 time steps, i.e. 0.5 nondimensional time, at the normal position of C in Fig.2 corresponding to the maximum mean velocity. It is observed that, when streamwise and spanwise distances increase, the two-point correlation coefficients of u, v and w decrease rapidly. In fact, when the the two-point distance is greater than 1.5, say, the velocity correlations are negligible. Thus, the computation domain employed here is large enough to resolve large-scale structures in the flow.

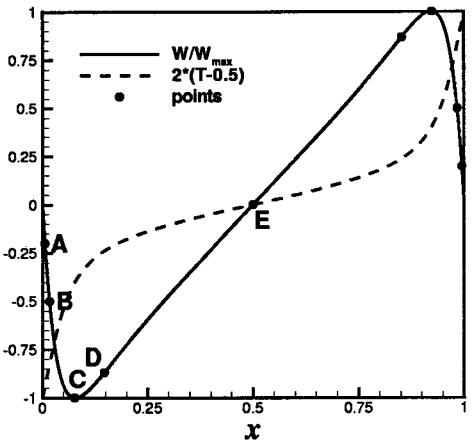

Figure 2: Mean velocity and mean temperature distributions of the thermal convection flow ($Pr = 0.71$,$Ra = 5.4 \times 10^5$).

CHARACTERISTICS IN FREQUENCY AND WAVE-NUMBER SPACE

For the natural convection of the second kind, the characteristics of the flow are strongly affected by the walls. From the mean velocity profile shown in Fig.2 the flow can be roughly devided in two parts: the wall flows at $x < 0.075$ and $x > 0.925$ and the Couette flow in the region $0.075 < x < 0.925$. Shown in Fig.2 are five points on the mean-velocity profile at different normal positions from the cold wall. Spectrum characteristics of the flow are analyzed using the data of these five points. The distances to the cold wall of these five points from A to E are respectively $y^+ = 0.7$, $y^+ = 2$, $y^+ = 9.4$, $y^+ = 18.2$ and $y^+ = 61.6$, where $y^+ = u^* y/v$ with $u_* = 87.5$. At the positions of point B near the cold wall and point E in the central region, the power spectra of the fluctuating velocities of u', v' and w' are in frequency space (Fig.4). It is observed here that near the wall the power spectra exhibit strong anisotropy at all frequencies and the energy associated with the vertical fluctuating velocity u' is much less than the spanwise v' and streamwise w' components. The streamwise velocity w' has higher energy than v' at both lower and higher frequency regions. At E point in the center between the two walls, there is a good collapse of power spectrum data between v' and w' over all the scales. In fact, the normal component also comes close to the v' and w' spectral curves at high frequencies indicating good turbulence isotropy at small scales. But at the energy-containing large scales the power spectrum of u' is significantly lower than those of v' and w'. This contributes to the overall anisotropy between u' and v', w'. This general anisotropy in the central zone is one of the main reasons that the current turbulence models have difficulties to resolve this type of flow.

The energy spectrum curves in spanwise and streamwise wave number space for points A, B, C, D, E are plotted in Fig.5. It is observed that turbulence is most energetic towards the center of the flow and this is consistent with the distribution of time average of the fluctuating kinetic energy shown in Fig.6. The turbulent kinetic energy is denoted as $e = 0.5 < u_i' u_i' >$ in this paper. It is seen that e increases

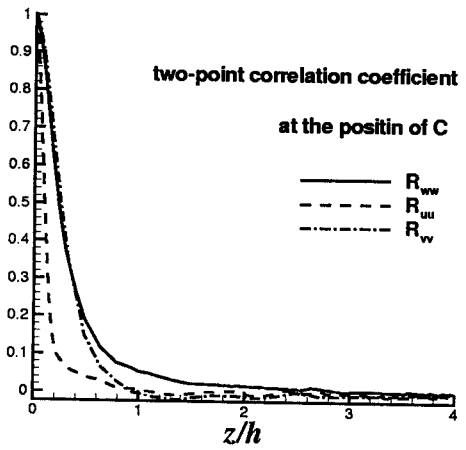

(a)

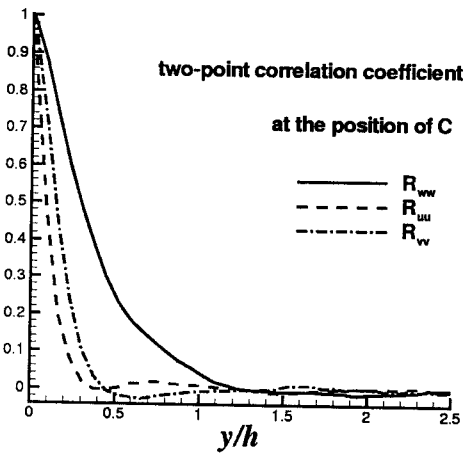

(b)

Figure 3: Statistically-averaged two-point correlation coefficients in streamwise and spanwise directions at the normal position of C in Fig.2.

with the distance to the center of the flow. The energy spectra at these five positions have similar shapes. When $k_y, k_z \approx 0.7$, the energy spectra reach maximum values. It may thus be conjectured that the characteristic length scale of the large-scale structures is approximately $1.4h$ in both the spanwise and streamwise directions. At larger wave numbers, from 2 to 10 say, the flow is in the inertia sub-range similar to what Komogorolv theory has described. Their slopes in logarithmic coordinate are all approximately -5/3. At the wave numbers larger than about 20, energy spectra decrease much slower, there is even spurious increase in the data at point D and E. The spectra is likely in the dissipation range, but another possible reason is that the limited mesh number makes energy spectrum distorted.

The time series of the fluctuating kinetic energy at points B, D and E are transformed to frequency space with FFT. The energy spectrum curves are plotted in Fig.7. It is seen that the energy spectrum reaches maximum value at $f \approx 100$ and the large time scales are in the range $t_L = 0.01 - 0.1$. At larger frequencies, about from 400 to 4000, the flow is in the inertia subrange with slopes in logarithmic coordinate at approximately -5/3. The curves for points D and E come very close indicating the flow structures in the Couette-flow

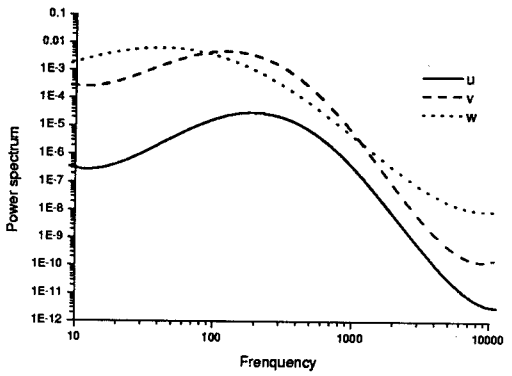

(a)

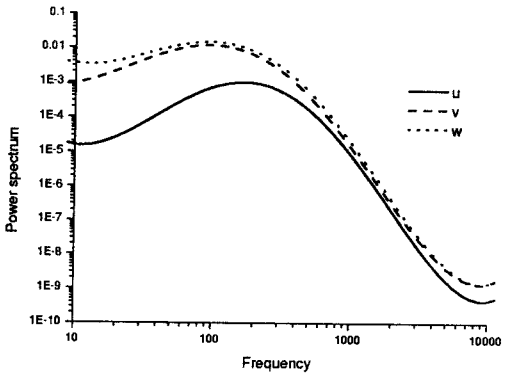

(b)

Figure 4: Power spectrum in frequency space of u', v' and w' of B point(a) and E point(b).

region are similar. The energy spectrum very near the wall (point B) is significantly lower than those at points D and E especially at large scales. This is understood as the wall inhibits large scale turbulent motions.

It is generally seen here that energy spectra of the flow quantities consist typically two regions, the energy-containing region and the inertia region. The characteristic large time scales with high energy spectrum are between 0.01–0.1, and the large length scales in y and z directions is around 1.4h. This is in accordance with the characteristics of the large-scale structures described in the following text. In the inertia sub-range, -5/3 law can be violated in the near wall region due to strong anisotropy of the flow. Due to the resolving power, the energy-dissipation region in the present computation is not evident. Finer grid mesh may be required.

FLOW PATTERNS AND LARGE-SCALE SPIRAL STRUCTURES

In the present study a major observation is the presence of spiral structures in the flow (Wang *et al* 2002). In order to have an intuitive impression of the flow patterns, Fig.8 shows some instantaneous streamlines passing through the high-helicity regions near the walls. These flow structures are then examined with their projections on a series of planes perpendicular to the z-axis (mean streamwise) and x-axis (normal to the walls) respectively. For examples, Fig.9 and Fig.10 show such projections in which domains enclosed with a dash-dotted square box correspond to the flow struc-

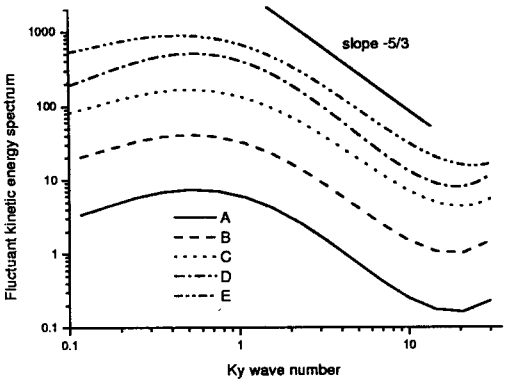

(a)

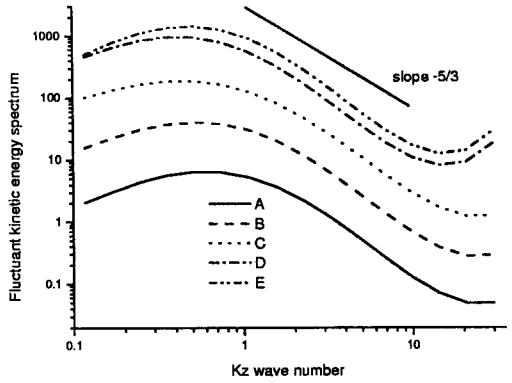

(b)

Figure 5: Fluctuant kinetic energy spectrum in spanwise(a) and streamwise(b) wave number space of A, B, C, D and E with different wall distances respectively.

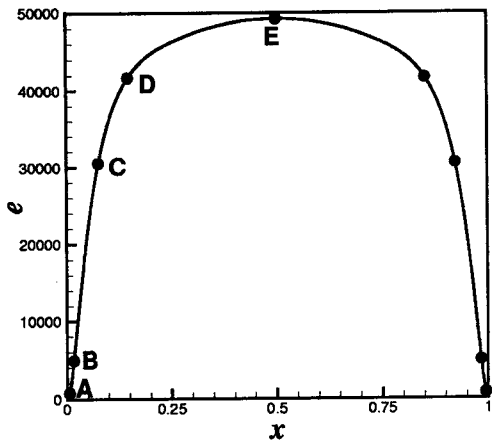

Figure 6: The distribution of average turbulent kinetic energy with the vertival coordinate x.

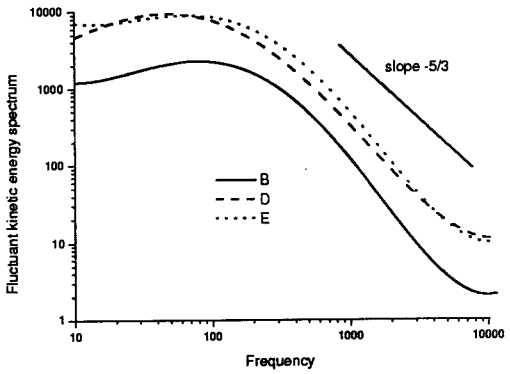

Figure 7: Fluctuant kinetic energy spectrum in frequency space of B, D and E points

ture of Fig.8(a). It is seen in Fig.9 that the spiral structure originates at the plane $z = 0$ near the cold wall. At the plane z=0, which is the bottom cross-section of the computational domain, a pair of spiral singularities exist, one being inside the square box and the other outside. These two singularities wind up to form an asymmetric counter-rotating vortex pair at the plane $z = 0.3$. Meanwhile, at the plane $x = 0.07$ very close to the cold wall, a singularity of skew divergent node in the square box can be observed in Fig.10. This singularity node is strongly characterized by the upward velocity component in z-direction against the general downward motion of the fluid outside the singularity region due to buoyancy effect. The strong upward motion generates large shear rates around the singularity node causing this node singularity to develop to a spiral singularity which becomes evident at the plane $x = 0.2$. Further away from the cold wall, i.e., at the plane $x = 0.4$, a pair of asymmetric counter-rotating vortices form with one of them inside the square box as shown in Fig.10. Upwards in z-direction, as $z = 0.3 \sim 1.2$, the vortex of the counter-rotating pair outside and below the square box (see Fig.10) becomes weaker and weaker and disappears eventually. As the spiral flow reaches a position near the hot wall, the strength of the vortex highlighted in the square box degenerates again to a divergent-node singularity (see Fig.10 for the plane $x = 0.93$) denoting a transverse velocity component in x-direction. Fig.9 thus illustrates that the spiral structure in Fig.8(a) stretches mainly upwardstilting from the cold wall to the hot with an angle of about 21.2 degree.

The cause of the spiral structure from generation to disappearance is interesting and important for the investigation of its mechanism. The time evolution of the spiral structure shown in Fig.8(b) is illustrated in Fig.11, where t_{ST} is the starting time for observation, $\Delta t = 5 \times 10^{-5}$ is the non-dimensional time increment in the DNS computation. The procedure to find such a time series is first to identify a mid-life structure shown in Fig.11(d) through searching the field values with large relative helicity at a particular instance. Then, the flow streamlines are plotted before and after this time until the spiral streamlines disappear. This figure thus illustrates that the lifetime of such a large-scale spiral structure is about of the same order of the global time scale defined by the characteristic length h and the friction velocity u_* ($u_* = \sqrt{\tau_w/\rho} \approx 0.011$, $\tau_w = \mu(dW/dx)\,|_{wall}$). The lifetime of the helical flow pattern is equivalent to the time interval in which the flow preserves its topological structure. It is seen that this time interval is at least two orders of magnitude longer than that of small-scale turbulent structure.

ROLE OF HELICITY IN PRESERVING THE SPIRAL STRUCTURES

It has been suggested (Tsinober and Levich(1983), Mof-

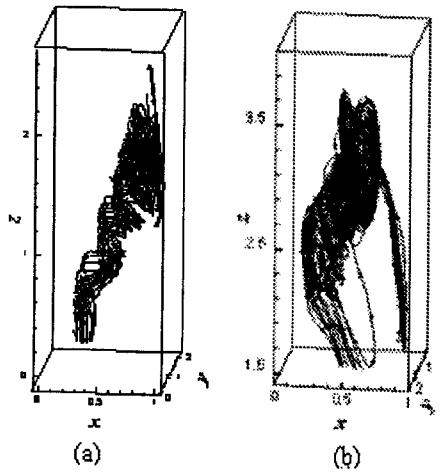

Figure 8: Isolated instantaneous spiral structures corresponding to the high helicity regions near the plate ($Pr = 0.71, Ra = 5.4 \times 10^5$), which appear in different moments, and the center points of the starting section of the structures are located respectively about at the coordinates of (0.95, 1, 2.4), (0.8, 2.2, 0).

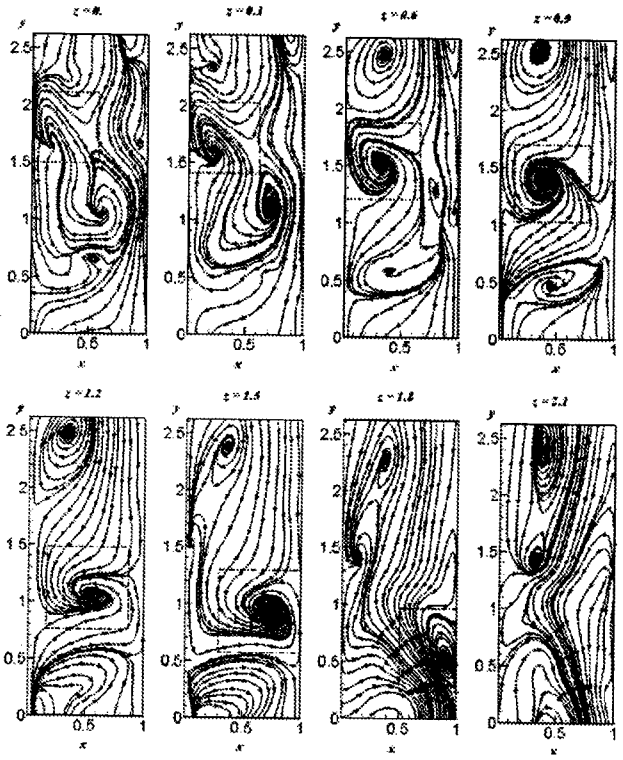

Figure 9: Projections of the flow pattern on the planes perpendicular to the z-axis. Domains enclosed with dash-dotted squares correspond to the structure given in Fig.8(b).

fatt(1984)) that the fluctuations of helicity play an important role in the non-linear dynamics of complex flows and is likely directly related to coherent structures in turbulence. Helicity (strictly speaking helicity density) H is defined as the scalar product of the velocity and vorticity vectors, i.e. $H = \vec{u} \cdot \vec{\omega}$, where $\vec{\omega} = \nabla \times \vec{u}$, relative helicity is called h, i.e. $h = H/(\mid \vec{u} \mid\mid \vec{\omega} \mid) = cos\theta$, where is θ the angle between the velocity and vorticity vectors. Both H and h are pseudoscalar quantities since they change signs if the frame of reference changes from a right-handed co-ordinate system

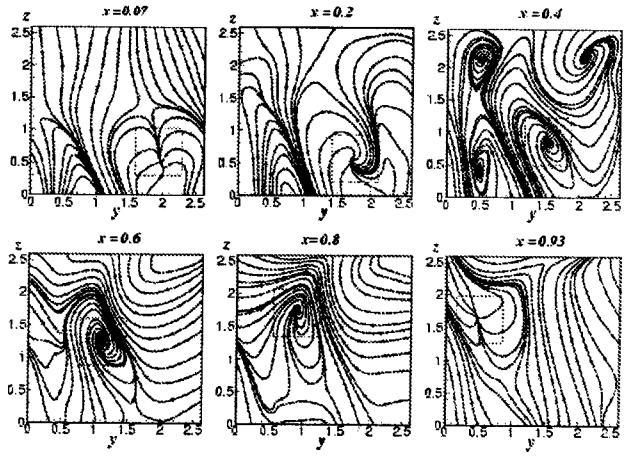

Figure 10: Projections of the flow pattern on the planes perpendicular to the x-axis. Domains enclosed with dash-dotted squares correspond to the structure given in Fig.8(b).

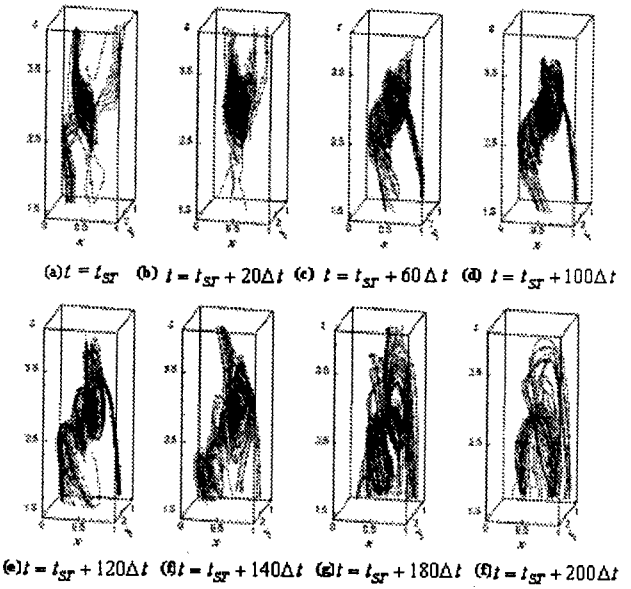

Figure 11: Evolution of a spiral structure with time, $\Delta t = 5 \times 10^{-5}$ is the time step normalized by h^2/κ. ($Pr = 0.71, Ra = 5.4 \times 10^5$)

to a left-handed one, in other words, H and h are quantities lacking parity-invariance.

Helicity of the flow has an intrinsic property to suppress dissipation. A simple explanation is as follows. The Boussinesq equation (2) can be re-written in its vectorial form as

$$\frac{D\vec{u}}{Dt} - \vec{u} \times \vec{\omega} = -\nabla(\frac{p}{\rho} + \frac{\vec{u} \cdot \vec{u}}{2}) + \nu \nabla^2 \vec{u} + \beta g(T - T_0)\vec{e_3} \quad (4)$$

where $\vec{e_3}$ is the unit vector in the vertical z-direction. In Eq.(4), the only nonlinear term that exchanges energy between different scales is the Lamb vector $\vec{u} \times \vec{\omega}$. This term is related with the relative helicity by an identity

$$\frac{\mid \vec{u} \times \vec{\omega} \mid^2}{\mid \vec{u} \mid^2 \mid \vec{\omega} \mid^2} = 1 - h^2 \quad (5)$$

Thus, in a flow region with high helicity the amplitude of the Lamb vector $\vec{u} \times \vec{\omega}$ is correspondingly low, and hence the energy exchange between different scales becomes less significant. Generally speaking, in a high Reynolds number

flow the viscous dissipation of energy-containing scales can be negligible. The removal of the energy of these scales is due mainly to nonlinear interaction and cascade behaviour. This explains why a strong helical flow structure on a certain scale can preserve its energy and survive much longer than a non-helical one.

Furthermore, if the energy cascade is suppressed by the effect of helicity, the viscous dissipation of the smallest scale would also be reduced. Thus, a flow region with high helicity values is conjectured to correspond to that of low dissipation. The relationship between the helicity and the dissipation rate can be further elucidated by plotting the helicity directly against the dissipation rate as shown in Fig.12. Fig.12(a) clearly shows that for the spiral flow indicated in Fig.8(b), high helicity magnitudes are closely associated with the low dissipation values. Fig.12(b) is a similar plot but with the conditional averaging over 50 equally spaced intervals in $\epsilon'/\epsilon'_{max}$. These plots confirm the conjecture metioned above. The other structures are also analyzed in similar ways, the same conclusion has also been drawn.

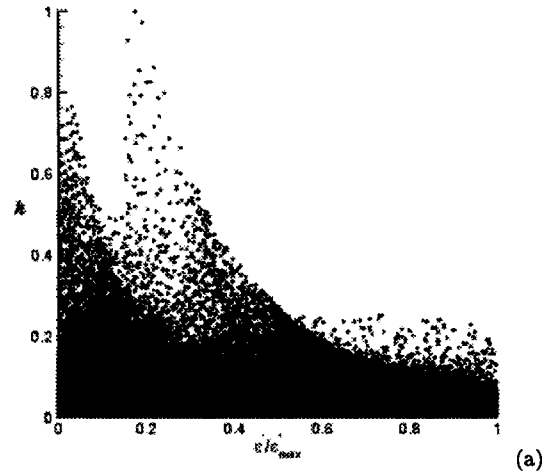

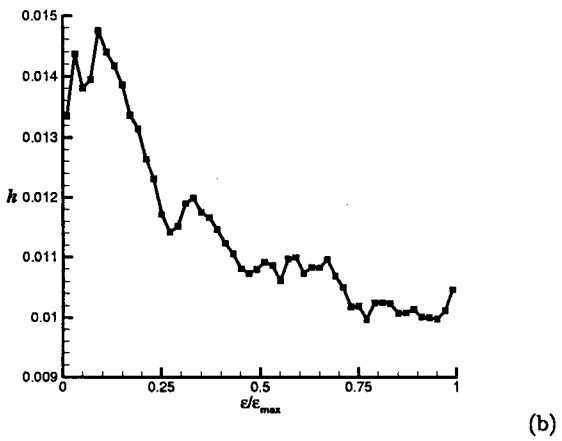

Figure 12: (a) Dissipation rate and absolute value of relative helicity in the instantaneous flow region same as fig.8(b); (b) Conditional average of relative helicity conditioned upon dissipation rate for all the computational points. Average of absolute value of relative helicity for 50 divisions from 0 to 1 with the width of 0.02 is computed for the points whose ϵ' belong to those zones.

CONCLUSION

By means of studying the correlation coefficients in homogeneous directions, it is shown that the computation domain is large enough for the study of the large scale structures. Through FFT technique, flow characteristics in frenquency and wave number space are analyzed. The power spectra of u', v' and w' at the different normal positions indicate that turbulence anisotropy in this type of natural convection at Ra= 5.4×10^5 exists generally even away from the wall at the center between the plates. But the difference between the energy components in the two homogeneous directions is negligibly small. The energy spectrum curves exhibit two typical regions, the energy-intensive and the inertia regions. The dissipation region is eveident. The characteristic large time scale with high energy spectrum ranges from 0.01 to 0.1, and large length scale in y and z directions is around 1.4h.

It is observed that the turbulent flow induced by the thermal convection between two differentially heated vertical plates can generate large-scale spiral structures. The instantaneous flow patterns and time evolution of this kind of structures are plotted. The observed length scale and lifetime of such spiral structures is in accordance with the spectral results. The role of helicity in the flow is to suppress the energy cascade of turbulence, reducing the dissipation, and hence preserving the topological structure of the large-scale spiral flow for a significantly long time interval.

REFERENCES

Boudjemadi, R., Maupu, V., and Laurance, D., 1997, "Budgets of turbulent stresses and fluxes in a vertical slot natural convection flow at Rayleigh number $Ra = 10^5$ and $Ra = 5.4 \times 10^5$", *Int. J. Heat and Fluid Flow*, Vol. 18, pp. 70-79.

Cortese, T., and Balachandar, S., 1993, "Vortical nature of thermal plumes in turbulent convection", *Phys. Fluids A*, Vol. 5(12), pp.3226-3232.

Dafa'Alla, A. A., and Betts, P. L., 1996, "Experimental study of turbulence natural convection in a tall cavity", *Exp. Heat Transfer*, Vol. 9, pp. 165-194.

Moffatt, H. K., 1984, *in Turbulence and Chaotic Phenomena in Fluids*, Elsevier, New York, pp. 223-230.

Phillips, J. R., 1996, "Direct simulations of turbulent unstratified natural convection in a vertical slot for $Pr = 0.71$", *Int. J. Heat Mass Transfer*, Vol. 12, pp. 2485-2494.

Ruth, D. W., 1979, "On the transition to transverse rolls in an infinite vertical fluid layer - a power series Solution", *Int. J. Heat Mass Transfer*, Vol. 22, pp. 1199-1207.

Tsinober, A., and Levich, E., 1983, "On the helical nature of three-dimensional coherent structures in turbulent flows", *Phys. Letts.*, Vol. 99A, pp. 321-323.

Versteegh, T. A. M., and Nieuwstadt, F. T. M., 1997, "Coherent structures in natural convection between two vertical, differentially heated walls", *Proc. International Symposium on Turbulence and Heat and Mass Transfer*, Delft.

Versteegh, T. A. M., and Nieuwstadt, F. T. M., 1999, "A direct numerical simulation of natural convection between two infinite vertical differentially heated walls - Scaling laws and wall functions", *Int. J. Heat Mass Transfer*, Vol. 42(19), pp. 3673-3693.

Wang, Minhao, Fu Song, and Zahng Guanghua, 2002, "Spiral plume structures in turbulent natural convection between two vertical walls", *Chinese science Bulletin, 2002*, Vol. 47(11), pp. 955-959.